

Principal component analysis of *IUE* galaxy spectra

Liliana Formigini and Noah Brosch

*The Wise Observatory and the School of Physics and Astronomy
Raymond and Beverly Sackler Faculty of Exact Sciences
Tel Aviv University, Tel Aviv 69978, Israel*

Accepted 2003 MMM DD, Received 2003 MMM DD, in original form 2003 MMM DD

ABSTRACT

We analyse the UV spectral energy distribution of a sample of normal galaxies listed in the *IUE* INES Guide No. 2-Normal Galaxies (Formigini & Brosch, 2000) using a Principal Component Analysis.

The sample consists of the *IUE*-SW spectra of the central regions of 118 galaxies, where the *IUE* aperture included more than 1 per cent of the galaxy size. The principal components are associated with the main components observed in the UV spectra of galaxies. The first component, accounting for the largest source of diversity, can be associated with the UV continuum emission. The second component represents the UV contribution of an underlying evolved stellar population. The third component is sensitive to the amount of activity in the central regions of galaxies and measures the strength of star formation events.

In all the samples analysed here the principal component representative of star-forming activity accounts for a significant percentage of the variance. The fractional contribution to the SED by the evolved stars and by the young population are similar.

Projecting the SEDs onto their eigenspectra, we find that none of the coefficients of the principal components can outline an internal correlation or can correlate with the optical morphological types. In a sub-sample of 43 galaxies, consisting of almost only compact and BCD galaxies, the third principal component defines a sequence related to the degree of starburst activity of the galaxy.

Key words: :galaxies:fundamental parameters-stellar content-ultraviolet:galaxies - methods:data analysis

1 INTRODUCTION

The history of UV astronomy shows that (a) only a few missions operated and yielded significant data, and (b) most of these missions dealt with imaging or photometry, with very limited spectral science. Among the latter, the *IUE* project stands out with more than 18 years of successful operation and with a yield of more than 10^5 spectra collected and uniformly analyzed. These spectra have been available on-line in the *IUE* final archives and through the various astronomy data portals. The compilations from the *IUE* data base offer a somewhat biased view of the UV spectral characteristics of astronomical objects. In particular, the INES Guide No. 2 “Normal Galaxies” (Formigini & Brosch 2000) offers a view of the UV spectral characteristics of the non-active galaxies.

The advent of the *GALEX* all-sky UV survey, with a strong component of spectral science (Bianchi et al. 1999), argues for the development of new tools to understand the spectral energy distribution of galaxies in the UV. While traditionally UV spectra have hardly been used for classification, partly because of the lack of a large number of spec-

tra of different objects, it is possible that the $\sim 10^5$ galaxy spectra expected from *GALEX* would provide the necessary data base to develop an independent and uniform classification network using only UV information.

The question we posed ourselves was whether it is possible to predict the UV spectrum of a galaxy by using exclusively information from the optical domain. The question is relevant in the context of UV surveys, when one needs to estimate the spectral detections, and also when one deals with huge data bases derived from a survey of a large fraction of the sky.

In the optical domain, the Hubble diagram provides a satisfactory classification for local galaxies, with redshift ≤ 2 , based on their appearance. This morphological classification however, is a qualitative and somehow subjective analysis of the observable features of a galaxy. Classification of several hundreds of galaxies, performed by different experts (Lahav et al. 1995), results in a dispersion of more than one morphological type. For irregular and peculiar galaxies the situation is worse, because the Hubble classification does not define if an irregularity or peculiarity is related to shape,

such as asymmetry, or to surface brightness, such as the lack of a central concentration.

Morphological classification depends also on the photometric filter. The appearance of galaxies in the UV is different from that in the optical, and details emphasized in the UV often do not agree with the Hubble classification. For instance, UV images of spiral galaxies show detailed features in the spiral arms and in the bulge, such as knots of circumnuclear star-formation regions, that cannot be clearly detected in the optical band. Low redshift UV galaxies are important both for understanding the local Universe and for the extrapolation to high redshift samples,

However, the higher percentage of irregular and merger types found in high redshift samples (Brinchmann et al. 1998) indicates that the Hubble sequence is not sufficient to describe the complex UV morphology. Kuchinski et al (2000) analyzed a sample of 34 nearby galaxies imaged with UIT, and found that the far-UV morphology does not agree with the bins of the Hubble sequence. The introduction of two additional parameters, to quantify the asymmetry and the central concentration of galaxies, is suggested by Kuchinski et al (2001).

Classification can be performed also using the spectral energy distribution (SED). Galaxies of the same morphological type tend to have similar stellar populations and this results in similar spectral features in the optical domain. Hence, a spectral classification based on the SED is related to the physical properties of a galaxy, such as its stellar and gas content. An objective method for spectral classification is the Principal Component Analysis (PCA), extensively applied to samples of templates and to galaxy models. This technique was able to retrieve regularities present in the optical spectra and to define a spectral sequence for normal galaxies (Connolly et al. 1995; Sodr  & Cuevas 1997; Galaz & de Lapparent 1998; Ronen, Aragon-Salamanca & Lahav 1999).

In this paper we analyse a set of UV spectra of galaxies from the *IUE* final archive. This archive represents the most extended UV database on galaxies until new systematic UV surveys from space, such as that by *GALEX*, will be available. We use the INES Guide No.2-Normal Galaxies (Formigini & Brosch, 2000)*.

A large effort has been expended in studying the *IUE* spectra of galaxies by Bonatto, Bica & Alloin (1995) and Bonatto et al. (1996, 1998, 1999), by grouping the galaxies presenting spectral and optical morphological similarities and coadding the spectra in order to produce high signal-to-noise template spectra for subsets in each group.

In this work we analyse a set of direct spectra of galaxies, without attempting to build a-priori templates. The only selection criterion adopted is the coverage parameter, defined in section 2. This parameter evaluates the area of the galaxy included in the *IUE* spectrograph aperture. The PCA method is described in section 3. In section 4 we discuss the PCA results, and the effect of normalization on the sample and on a subset with good signal-to-noise. A data set with spectra covering a higher fraction of the galaxy is also

analysed, and the Hubble optical morphological sequence is compared to the UV spectral sequence in section 5.

2 THE *IUE* SAMPLE

A suitable set of UV SEDs of galaxies covering a wide range of Hubble types can be extracted from the *IUE* final archive. The data sets provided by INES (*IUE* Newly Extracted Spectra) consist of low-resolution spectra extracted with an improved method from the line-by-line images of the *IUE* Final Archive, and of high-resolution spectra resampled to the low-resolution wavelength step. A collection of UV spectra of 274 normal galaxies has been compiled as the INES Guide No. 2 (Formigini & Brosch 2000). In this guide, a representative UV spectrum for each galaxy has been selected, combining the longest short-wavelength (SW) and long-wavelength (LW) exposures of the galaxy, both taken through the large aperture. The aperture position of the *IUE* apertures for the SW and LW spectra, that were obtained independently and required repositioning of the satellite, were checked with aperture overlays on the galaxy images. This procedure assured that the entrance apertures of both SW and LW spectra were centered on the galaxy optical position or, alternatively, refer to same physical region of the galaxy, such as the HII regions of NGC4449 and NGC5236.

We found some cases where the *IUE* aperture coordinates did not correspond to the coordinates of the galaxy, and the *IUE* did not, in fact, observe the object. Such is, for instance, the *IUE* spectrum of NGC 3077, where the misplaced aperture contains a foreground star instead of the galaxy.

The large apertures of the *IUE* spectrograph are 10"×20" ovals, each corresponding in area to a circular diaphragm with a diameter of 15.1 arcsec (Longo & Capaccioli 1992), and many of the galaxies observed are extended with respect to these large apertures. In order to estimate the fraction of the galaxy area observed by *IUE*, we calculated for each galaxy the "coverage parameter" *C*, defined as the logarithmic ratio between the surface area of the galaxy and the area of the large *IUE* aperture.

$$C = \log[\pi \times (D_{25}^2 \times R_{25}) / (15.1)^2 \pi / 4] \quad (1)$$

Here *D*₂₅ and *R*₂₅ are the major axis and the axial ratio of the optical image of the galaxy as listed in NED, in units of arcsec. The numerator approximates the surface area of the galaxy, represented as an ellipse with the major and minor axes of the galaxy.

A *C* value of zero implies that the entire galaxy was measured by the *IUE* spectrum. For faint galaxies, where the axes are not measurable, the *C* parameter is ≤ 0 . The histogram of the number of galaxies as a function of the *C* parameter (see Figure 5 of Formigini & Brosch, 2000) shows that, for 90 per cent of the sample of 274 normal galaxies in the INES Guide No.2, the *IUE* aperture covered less than 10 per cent of the galaxy.

For the present investigation, only the galaxies with a *C* value up to 2, corresponding to a coverage of more than 1 per cent of the galaxy were assembled from the sample of Formigini & Brosch (2000). This means that the spectra are dominated by the content of the very center of the light distribution of the galaxy. A few cases where the aperture

* Retrievable electronically at
http://wise-iue.tau.ac.il/~lili/Fnet/Fnet.html

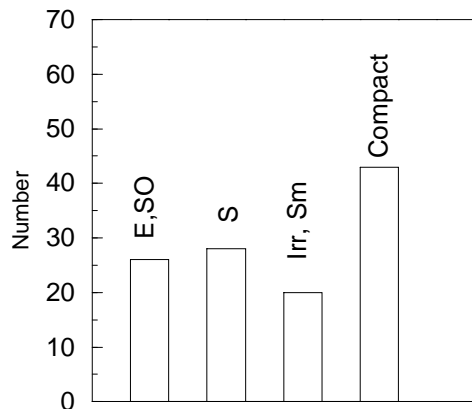


Figure 1. The distribution of spectral types

position was miscentered were rejected. The total number of galaxies included in the sample analyzed here is 118. Table 1 lists the relevant data for the set. Column two indicates to which sub-sample the specific galaxy belongs, where 1 represents membership in the sub-sample of relatively high S/N and 2 represents membership in the sub-sample of high coverage parameter (see section 4). This sample, resulting from many different research projects, contains galaxies of all morphological types, although it is obviously biased toward the brightest UV galaxies. It is a representative sample of UV galaxy spectra although it is not uniform, and the percentage of galaxies in each morphological class is not representative of the galaxy population at large. Consequently, this sample is not suitable for luminosity function and density investigation. A sub-sample of galaxies with C values up to 1, corresponding to a coverage of more than 10 % of the galaxy area, was selected for comparison. This reduced sample of 43 galaxies, consisting mostly of BCD and compact objects, is analyzed in section 4.2.

Figure 1 shows the morphological distribution of the data set. The galaxies have been binned in four morphological bins: ellipticals, spirals, irregulars, and a group containing all the compact objects, namely galaxies classified as BCD, EmLS, HII and compact. Note that the morphological types and redshifts adopted here are from NED, while in the INES Guide No. 2 all information is from LEDA. The sample includes all classical Hubble types, from elliptical to irregulars, and a large proportion of compact/BCD/EmLS galaxies whose emission in the UV band is dominated by young, UV bright stars.

The redshift distribution of the sample is shown in Figure 2. *IUE* observed galaxies only in the very nearby Universe, hence the sample analyzed in this paper can be considered as representing the local UV galaxy population. This sample can be used to directly analyze the rest-frame UV SED of galaxies without requiring extrapolation from the optical data.

It is known that the galaxy spectra have a low signal-to-noise ratio in the *IUE* LW region. Actually, a visual inspection of the spectra in the LW range, shows that the noise is the dominant feature. Furthermore, only part of the galaxy sample has been observed in the LW range. Hence, we have restricted the analysis to the far-UV region covered by the SW *IUE* images (between 1150–1900 Å). This is the wave-

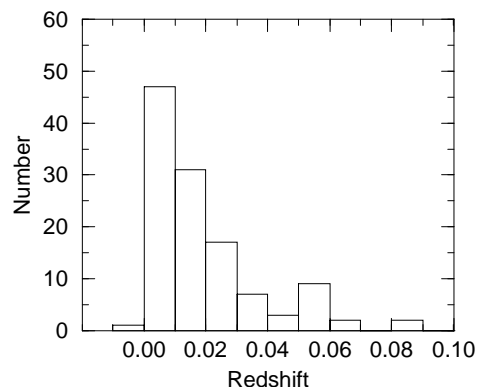


Figure 2. Histogram of the redshifts distribution

length range where the most significant features probing the galaxy evolution occur.

3 THE PCA METHOD

The technique used to analyze the UV spectra of our sample is the Principal Component Analysis (PCA; Whitney 1983). The PCA algorithm is an orthogonal transformation that, given a set of measured quantities, finds a set of new independent variables, called the principal components (PC), each one being a linear combination of the original quantities. PCA has been demonstrated to be a useful tool for spectral classification of both stars (Ibata & Irwin 1997; Singh, Gulati & Gupta 1998) and galaxies (Connolly et al. 1995; Ronen et al. 1999). It has been applied to quantities measured from the spectra, such as broad-band colors or equivalent width of lines (Turler & Courvoisier 1998; Steindling, Brosch & Rakos 2001), and also directly to the spectral energy distribution (SED) of galaxies (Sodré & Cuevas 1997; Galaz & de Lapparent 1998).

In spectral PCA, each spectrum is a vector in a multidimensional space, and the fluxes in the individual wavelength bins represent the axes of this space. PCA identifies the directions of the maximum variance of the spectral components. These directions, called principal components, are identified sequentially and represent the new axes that parameterize the volume spanned by the dataset. The principal components are ordered according to the fractional sample variance for which they account, the first component accounting for the largest fraction. If there are common characteristics between the galaxy spectra of the sample, a few principal components may account for a large fraction of the total sample variance. Therefore, the PCA, by reducing the multi-dimensionality of the data, may provide a simple description of the original dataset and, through this, a better insight on its underlying characteristics.

Each galaxy in our sample of *IUE* spectra is represented by a vector whose components are the M integrated fluxes in the individual wavelength channels. We consider a set of N vectors each of M elements $[X_{\lambda,i}, i=(1\dots,N), \lambda=(1\dots,M)]$, where N is the number of galaxy spectra. The sample is therefore represented by an $N \times M$ matrix. The eigenvectors of the covariance matrix are the new axes, called the prin-

principal components (PC), and the eigenvalues give their variance.

Since for PCA the spectra must be identically sampled in wavelength, and should have an equal number of bins, the *IUE* data have been preprocessed. Each spectrum has been dereddened for Galactic extinction using Seaton's (1979) law and shifted to the rest frame, according to the redshift data in Table 1. The SEDs have been corrected only for interstellar extinction, adopting a conservative approach. It is well-known that the Seaton standard extinction law is not suitable for external galaxies, and it sometimes overestimates the 2175 Å bump (Calzetti, Kinney & Storchi-Bergmann 1994, Calzetti 1999, Calzetti 2001). Moreover, the attenuation due to dust either within the galaxy or along its line of sight is an important effect in the UV range. This attenuation effect depends strongly both on the relative geometric distribution of dust and stars, and on the dust chemical composition or metallicity. A differential internal reddening law should be applied to each galaxy. However, we still have only a limited knowledge of the dust properties in the Milky Way and in the Magellanic Clouds, and of the differential extinction curve properties of quiescent and active-region galaxies (Gordon et al. 2003). Since the energy absorbed by dust is reprocessed, mainly in the infrared, an estimation of the extinction requires multiwavelength data or, at least, a measure of the infrared emission for each galaxy. In the future such data will become available thanks to the UV and IR surveys of GALEX and of SIRTf.

Our sample of galaxies is UV-selected, and we estimate that this ensures that the galaxy light is not heavily absorbed, although the presence of several dusty systems cannot be excluded.

Moreover, the ratio of the infrared to the far-UV emissions is different for different star populations. A dust-reddened population mimics an older unreddened stellar population: this could affect the interpretation of the relative contribution of each age population to the total galaxy spectrum. Bonatto et al. (1998, 1999) already noted that some galaxies have a contribution of young stars, although their spectrum looks very red. Spectral features, such as the line equivalent widths, can help distinguish a reddened population from an old one.

The use of a statistical approach, such as the PCA, limits the possibility of separating an older population from a reddened one and this should be considered when analysing the possible correlation (section 5) between principal components and the morphological galaxy types. We believe that although the mixing of morphological types can be partially attributed to differential dust absorption, our analysis indicates that the PCA methods applied to larger galaxy samples could be a useful classification method.

The redshift range spanned by the sample is small (see Fig 2), so that the wavelength range covered by all the galaxies of the sample is similar but slightly shorter than that covered by the SW *IUE* spectra. Note that in almost all galaxies, owing to the small redshift range, the NV $\lambda 1242\text{\AA}$ line is blended with the geocoronal Ly α .

The rest-frame spectra have been rebinned to a linear wavelength scale in the rest frame. The wavelength increment adopted is twice the sampling interval of the low-resolution SW spectrograph of *IUE* ($\simeq 3.4\text{\AA}$), in order to preserve the spectral features of each spectrum. This incre-

ment determines the number of wavelength points to be used for the PCA. Note that the *IUE* spectral resolution is much superior to that of GALEX ($\Delta\lambda/\lambda \simeq 150$), Bianchi and the GALEX team, 1999) offering, in principle, a better discriminating power.

The sample chosen for the present analysis is therefore represented by 118 galaxy spectra, each with 204 wavelength flux bins. The $N \times M$ matrix representative of the sample is a 118×204 singular matrix, and the eigenvalues of the covariance matrix were found using the singular valued decomposition technique (SDV: Mittaz, Penston & Snijders 1990). The average of the rest-frame, rebinned spectra has been subtracted from each spectrum. This procedure ensures that the dataset of the subtracted spectra should contain the maximal amount of discriminatory information. Otherwise, the average of the spectra dominates the matrix and the first principal component.

The problem of scaling and normalizing the input data before applying the PCA method has been extensively addressed (Francis et al. 1992, Connolly et al. 1995). For instance, the flux in each wavelength bin can be scaled to unit variance. The variance scaling is important when there are variables with a large range of absolute values, such as strong emission lines. The wavelength bins corresponding to these lines could dominate the PCA analysis and mask the continuum variations. Francis et al. (1992) found that the PCA results are insensitive to scaling and that the same number of components are present, although with different fractions of the total variance.

Connolly et al. (1995) analysed the effect of various normalization methods on the results of the PCA using a sample of template galaxy spectra. The most popular methods are the normalization by the integrated flux, or by the unit scalar product. The normalization by the integrated flux is not suitable for our sample, since it would give the same weight to high signal-to-noise as to low signal-to-noise spectra.

The alternative normalization method, by the scalar product, means that the sum of the squares of the (positive and negative) fluxes across the spectrum is forced to unity, $\sqrt{\sum X_{\lambda,i}^2} = 1$

Fig. 3 shows the mean spectrum of the 118 galaxies sample before and after applying the scalar product normalization. While the continuum trend is almost unchanged, the spectral features are smeared out by this normalization procedure.

Since our data are flux-calibrated spectra, and the total flux is an intrinsic characteristic of the galaxy, we applied the PCA analysis to the sample with no normalization and no scaling of the data. We compared the results with that of a normalised sample and of a sub-sample of galaxy spectra with good signal-to-noise, normalised by the scalar product.

4 THE PRINCIPAL COMPONENTS OF THE SAMPLE

In this section, the input data for our analysis are the fluxes in different wavelength bins, without variance scaling or flux normalization. The principal components are intrinsic to the spectra and can be related to both the magnitude and the

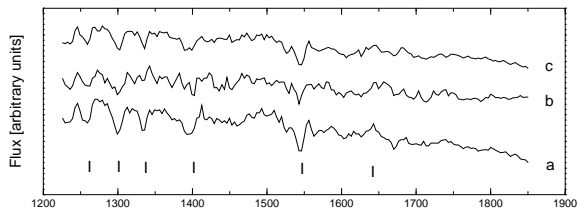


Figure 3. The mean spectrum of the sample without normalization (tracing a), after normalizing for the scalar product (tracing b), and after selecting for good signal-to-noise (tracing c). Tick marks indicates the following features: SiII $\lambda 1260$, OI $\lambda 1302$ plus SiII $\lambda 1304$, CII $\lambda 1335$, SiIV $\lambda 1400$, CIV $\lambda 1550$, HeII $\lambda 1640$

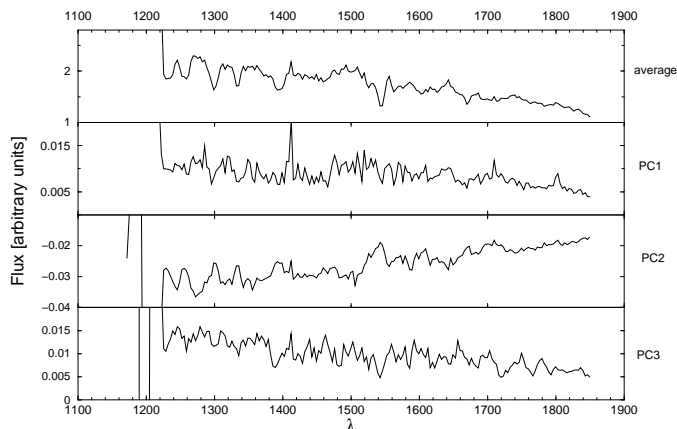


Figure 4. The average spectrum (top panel) and the principal components for the entire set. The three lower panels show the three principal components PC1, PC2, PC3.

features of the observed spectra (Folkes, Lahav & Maddox 1996).

The average spectrum (Fig. 4, top panel) shows no intense emission lines but only low and high ionization absorption lines, that can be both of stellar and interstellar origin. The most prominent absorption lines are the SiIV $\lambda 1400$ and the CIV $\lambda 1550$ doublets, which show a complex structure reminiscent of P-Cygni profiles. Additional low-ionization absorption lines of the blend of OI $\lambda 1302$ with SiII $\lambda 1304$, and of CII $\lambda 1335$, of both stellar and interstellar origins, are evident bluewards of 1400Å (De Mello, Leitherer & Heckman 2000). The emission feature at 1412Å does not seem to be a spurious feature introduced by noise. It could be the blend of SiIV $\lambda 1400$ with of SiIII $\lambda 1417$, a stellar photospheric line present in high-metallicity galaxies (Heckman et al. 1998).

The first three eigenvectors, shown in Fig. 4 together with the mean spectrum, account for 52 per cent, 17 per cent, and 14 per cent, respectively. These three eigenvalues carry 83 per cent of the information content of the total variance. Adding the fourth component, we account for up to 91 per cent of the variance. Subsequent eigenspectra contribute each a few per cent of the total variance.

The first PC (Fig. 4b) is flatter than the mean spectrum and modulations are present, such as the emission feature at $\lambda 1412$ as well as some absorption features such as the SiII/OI $\lambda 1300$ and the CII $\lambda 1335$ lines (Heckman et al. 1998). This PC component, accounting for the largest

variance of the data, represents the diversity from the average spectrum of the sample. It shows that a continuum ingredient flatter than the mean spectrum is the dominant component that characterizes each spectrum.

The second component (Fig. 4c) is flat at short UV wavelengths but shows a rising continuum redwards of the emission feature at $\lambda 1550\text{Å}$ with a residual of P-Cygni profile. This component represents the slope variation of the SED. It can be associated with the UV emission of the unresolved stellar population, such as individual stars and low luminosity stellar clusters (Calzetti, 1999), and it is correlated with the CIV $\lambda 1550$ emission.

The main feature of the third component (Fig. 4d) is the rising continuum blueward of $\lambda 1400$ towards the far-UV region, steeper than the mean spectrum. The modulation by the absorption lines of the SiIV $\lambda 1400$ and of CIV $\lambda 1550$ doublets is in the opposite sense to that shown by the PC2.

The rising UV continuum toward the far UV is recognized as a signature of the presence of young massive OB stars. These stars in which the emission peaks in the far UV, $\lambda \leq 1000\text{Å}$ represent, therefore, the bulk of the most recent or current starburst events in the galaxy. The strong winds of these stars originate the P-Cygni profiles seen in SiIV and CIV (Mass-Hesse & Kunth, 1998). Therefore, the third component represents the star formation activity and is correlated with the SiIV and CIV absorptions features.

The fractional variance accounted for by the 2nd and 3rd components is similar, showing that in our sample the contributions of the two continuum components, the young and the older stellar ones, are similar.

The fourth component (not shown here) is flat and shows only a weak signature of the HeII $\lambda 1640$ absorption/emission. This feature appears clearly only in the 6th and the 7th principal components that contribute only a few per cent (two and one) to the total variance.

4.1 The normalised sample

We applied the normalization by the scalar product to our sample of spectra and repeated the PCA analysis. The average spectrum of the normalised sample is dominated by the noise (see Fig. 3, tracing b) and many features are smeared out. In fact, this normalization process overweighs the poor signal-to-noise spectra in the sample and the resulting average spectrum depends on the percentage of good signal-to-noise spectra in the sample.

The principal components of the normalised sample are shown in Fig 5. It can be seen that the noise is so high that it hides all the spectral features. The first component accounts for only 36 per cent of the variance, the second one for 24 per cent, and the third for 13 per cent. Moreover, the spectral features of these components are anticorrelated with those of the average spectrum and are similar to each other. It seems that the PCA technique is unable to discriminate among the different contributions to the SED, as found for the non-normalised sample.

Folkes et al. (1996) found that in a noisy set of spectra the PCA method is still able to select the correlations in the fluxes at each wavelength, but few PCA components will be significant. Our result shows that the very noisy data and the statistical distribution of different spectral types in our sample make the normalization technique unsuitable.

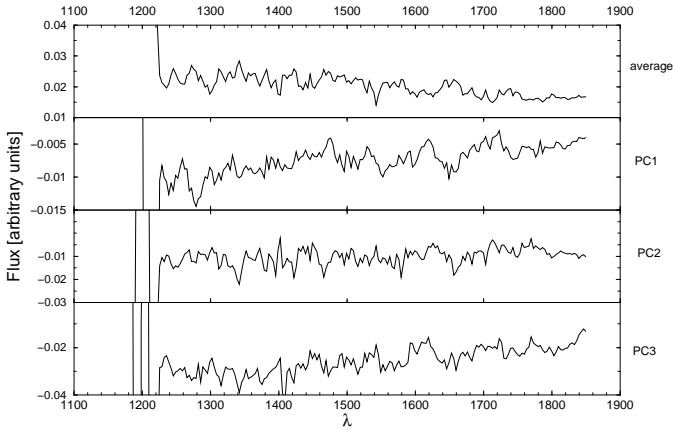


Figure 5. The average spectrum and the principal components for the normalised set

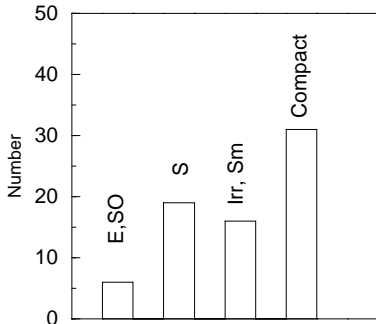


Figure 6. The distribution of spectral types for the good S/N sub-sample

The problem of signal-to-noise limitations of the *IUE* data can be overcome by grouping objects with similar spectra into morphological templates with high signal-to-noise. This binning procedure has been adopted, for instance, by Bonatto et al. (1995, 1996, 1998, 1999).

Instead of grouping the spectra a-priori, we performed a selection by signal-to-noise, and applied the PCA method to a sub-sample of relatively high-quality spectra ($S/N \gtrsim 3$) normalised by the scalar product. The average spectrum for this sub-sample of 76 galaxies is quite similar to that of the entire non-normalised sample (Fig. 3, tracing c). However, the two samples have a different morphological composition (Fig. 6). Selecting only spectra with good UV signal-to-noise has the effect of increasing the number of irregular/interacting systems, and the relative fraction of different galaxy types changes significantly. The elliptical galaxies are very poorly represented in this sub-sample, since their number drops from 28 to only 6 galaxies. While the fraction of BCD and compact galaxies remains almost the same, that of the elliptical ones changes from 24 per cent to 10 per cent.

The principal components for this sample are shown in Fig. 7, with the first component accounting for 41 per cent of the total variance, the second one for 23 per cent and the third one for 15 per cent. The first and, to a lesser degree, the second components show a redwards rising continuum that could represent the old stars' contribution to the total flux, while in PC3 the continuum is rising bluewards. In section

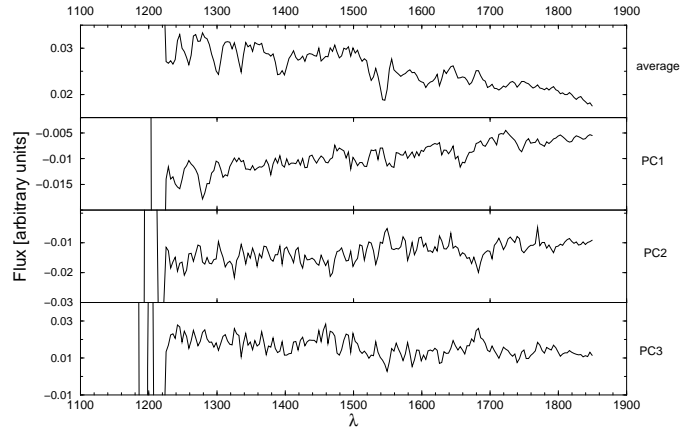


Figure 7. The average spectrum and the principal components for the normalised subset of good S/N spectra

5 we will correlate the PCA results with the morphological Hubble classification.

4.2 The reduced sub-sample

The PCA analysis was performed also for a sample of *IUE* galaxies having the "coverage parameter" (see section 2) up to 1. For this sample, the *IUE* aperture contained more than 10 percent of the galaxy. This sample consists of only 43 galaxies, mostly compact, BCD, and EmLS. Only four of the galaxies are normal ellipticals and spirals, and three are classified as irregulars. This sample is not representative of the galaxy morphology as a whole, but only of the compact and BCD classes.

Fig. 8 shows the principal components for this sub-sample, where PC1 accounts for 51 per cent of the variance, PC2 for 22 per cent, PC3 for 16 per cent of the variance, respectively. The first three components allow the reconstruction of the spectrum with an accuracy of 89 per cent.

The first principal component, flatter than the average spectrum, represents the residual continuum and measures how much each continuum spectrum differs from the mean one. The second one showing a rising continuum towards long wavelengths can be the emission of a residual population of A and F stars formed in previous bursts of star formation. Actually, the unresolved stellar population of a galaxy in which bright star-forming clusters, as well as small low-luminosity stellar clusters are embedded, contributes with a large percentage (50-80 per cent) of the UV emission (Calzetti, 1999). Note the anticorrelation with the high-ionization absorption lines of SiIV and CIV, formed in the expanding atmosphere of massive OB stars, that are a signature of active star-forming regions. The third component, characterized by a hard UV continuum and the SiIV and CIV lines in absorption, represents the starburst activity occurring in the galaxy.

5 SPECTRAL AND MORPHOLOGICAL CLASSIFICATION

The PCA analysis has already been applied to the study of integrated spectra of galaxies in the optical range. Connolly et

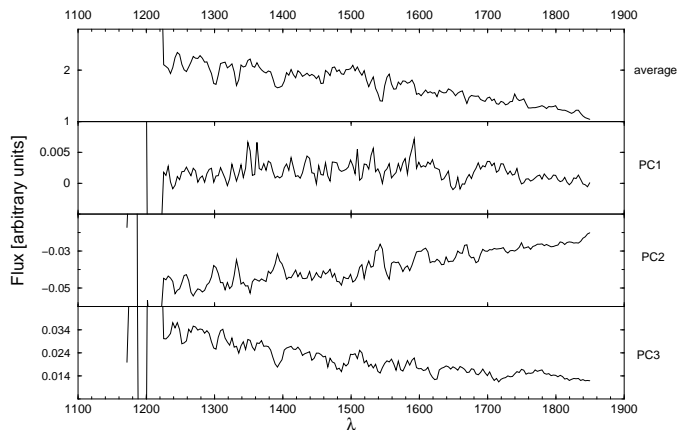


Figure 8. The average spectrum and the principal components for the sample with coverage factor up to 1

al. (1995) analyzed a template UV-optical spectral dataset that covers the range from 1200Å to 1μm finding that a linear combination of two eigenspectra describes adequately the galaxy spectral types. Folkes et al. (1996), and Sodr  and Cuevas (1994, 1997), applied the method to the Kennicutt spectrophotometric atlas of galaxies (Kennicutt, 1992) and to a sub-sample of normal galaxies. They found that the coefficients of the projection of the spectra onto the principal plane, i.e., the plane defined by the first and second principal components, define a spectral sequence. This sequence correlates with the Hubble morphological sequence, although there is an overlap between the different morphological groups.

The interpretation of the PCA analysis of the *IUE* spectra is more intriguing. We analyzed the coefficients of the projection onto the new orthogonal axes, i.e., the PC components, for each spectrum. These coefficients represent the contribution of each component to the overall spectral distribution of the galaxy. If there is an underlying global regularity responsible for the different kinds of spectra, these coefficients will show correlations and could be used to define some kind of spectral sequence in the UV.

For the analysis of the projected spectra, the galaxies have been binned in four morphological bins: elliptical, spiral, irregular, and a group containing all the compact objects, namely galaxies classified BCD, EmLS, HII, and compact. This class includes a variety of objects that show prominent UV emission, which can be explained by the presence of a central region of star formation.

It is usual to consider the diagram of the projections on the principal plane, since this is the plane that contains the maximal contribution to the variance (69 per cent, in our case). However, the projections on this plane fail to reveal any correlation and show only a large scatter. The plane defined by the first and the third eigenvectors represents nearly the same variance contribution (66 per cent) and here there is an indication of a sequence. Note that, as described in section 4, the third principal component represents the contribution of young stars to the SED, while the second one is the contribution of the underlying background of star forming activity that occurred in the past.

Fig. 9 shows the projections onto the plane defined by

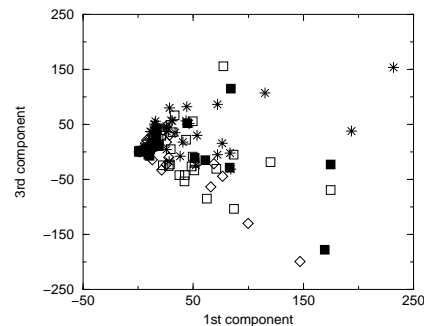


Figure 9. Projections onto the first and third eigenvectors of the spectra of the non-normalised sample. Filled squares indicate elliptical galaxies, open squares the spiral, diamonds the irregulars, and stars the BCD, HII and compact galaxies.

the first and the third principal components for the spectra of the non-normalised sample, after excluding a few unusual points. Although there is an indication of a sequence that follows a direction along the first component, there is also some vertical spread along the third component. In the plane defined by the second and the third components (fig.10) the elliptical galaxies and the compact ones lie on the same region apparently tracing a sequence, while the spiral and irregular ones show a large scatter. This could be interpreted as a similarity between the star formation activity of the nucleus of the elliptical galaxies and the compact ones.

The SED of early-type galaxies is often characterized by rising flux shortward of 1800 Å, known as the UV turnup. A mixture of low mass-stars on the horizontal branch evolutionary tracks is responsible for the UV flux (e.g., Brown et al. 1997). This turnup is mostly observed in galactic nuclei and could be significant in a sample of nearby galaxies observed throughout the *IUE* aperture, like this one. We cross-checked our sample with the Bica et al (1996) sample of elliptical galaxies finding only one galaxy in common, NGC4853, which does not present a UV turnup. A visual examination of the spectra of all the elliptical and SO galaxies of our sample reveals only a few galaxies with a moderate UV turnup: NGC1510, ABCG400A and ABCG1795. Deharveng, Boselli & Donas (2002), analysed the broad band UV-V and B-V colors for a sample of 82 galaxies, finding that only a minority of galaxies shows a strong turnup. Note also that signs of unusual activity have been found in the optical spectra of some early-type galaxies (Caldwell et al 1993), and residual starburst activity was also claimed by Deharveng, Boselli & Donas (2002) for some very blue elliptical galaxies. Although our sample is biased towards the UV brightest galaxies, it is hard to believe that almost all the elliptical galaxies of the sample show the same level of nuclear activity as the compact ones.

Fig. 11 shows the projection onto the plane defined by the first and the third eigenvectors of the spectra of the sample selected for good signal-to-noise and normalised by the scalar product (section 4.1). Here, the projections lie on an arc sequence, similar to the spectral sequence found by Connolly et al. (1995) for the ten templates of starburst and quiescent galaxies from Calzetti et al. (1994). Note that the curved sequence is due to the scalar product normalization, as already pointed out by Sodr  & Cuevas (1997). The

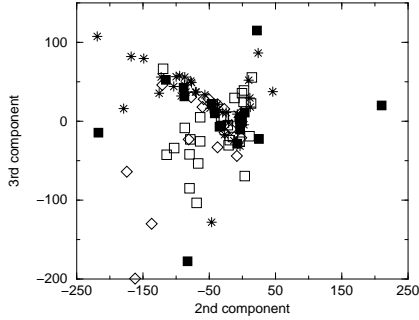


Figure 10. Projections onto the second and third eigenvectors of the spectra of the non-normalised sample. Filled squares indicate elliptical galaxies, open squares the spiral, diamonds the irregulars, and stars the BCD, HII and compact galaxies.

sequence is traced by the compact and irregular galaxies, but the binning with the morphological type is not unique. Spiral and elliptical galaxies are not segregated from other types and their location in the diagram shows that they are more consistent with a significant starburst component contribution to the SED.

The mixing of spectral types along the sequence is also evident in the projection of the components for the subsample of galaxies where more than 10 per cent of the galaxy area is included in the *IUE* entrance aperture (see section 4.2). In this sample, compact types are the dominant population and many of these galaxies are known to host one major central starburst region. Fig. 12a and 12b show the projections of the spectra onto the plane of the first and the third components and on the plane of the second and the third components, respectively. In both figures it is evident that the third component is able to trace a similar sequence populated by most of the compact galaxies, while the few spiral and elliptical galaxies in this sample lie at the bottom of the oblique trend, in a region of low values of the third component.

This trend is enhanced in Fig. 13, where the third component is plotted versus the average of the first and second orthogonal components. In this figure the galaxies can be separated into a group which follows a quasi linear and tight trend and a group with scattered large positive values on the horizontal axis. The ultracompact object Pox186 lies at the top of the sequence and the extremely metal-poor SBS 0335-052 and Tol 0420-414 lie at its bottom. The object at the top left-side of this figure is an HII region in NGC4449, while the irregular galaxy on the rising trend is IC2458 (Mrk 108), classified as BCD by Kinney et al (1993). The scattering at high positive values of the horizontal variable can result from the presence of dust. It is well known that the galactic extinction is not appropriate for correcting the attenuation by dust inside the galaxy. For instance, the point at the extreme right-side of Fig. 13 is Tol 0645-376 whose principal components are always unusual in all the diagrams. Terlevich et al. (1991) report a high $H\alpha/H\beta$ ratio of 4.28, larger than for Case B recombination, indicating that dust is present in the region of line formation.

It is not clear which is the physical parameter that defines the sequence. Pox 186 was believed to be the representative of an extreme population of isolated BCD galaxies at their first episode of star formation. Recently, an extended

halo feature was detected by Doublier et al. (2000). The colors of the outer region of the galaxy are consistent with an underlying evolved stellar population of late-K and M stars (Corbin & Vacca 2002), probably the residual of a previous mild episode of star formation. The UV image suggests the presence of two colliding clumps (Corbin & Vacca 2002), while there is no sign of this morphology in the optical image. Several bright star clusters have been detected at the centre of SBS 0335-052 (Papaderos et al. 1998) and also an extensive HI envelope. The observed properties make its classification as a young galaxy uncertain (Östlin & Kunth 2001). Similarly, in Tol 0420-414 a diffuse stellar component underlies the starburst, which is powered by Wolf-Rayet and O stars (Fricke et al. 2001).

It is becoming evident that not all the BCD galaxies are truly young objects (Kunth & Östlin 2000). For instance, the presence of an evolved population, formed at a continuous low rate or in a previous episode of star formation, is required to explain their broad-band colors (Gil de Paz, Madore & Perunova 2003). However, in starbursts the star formation knots dominate the entire galaxy emission, and only very large telescopes can detect halo structures.

In section 4.2 we argued that the third component is associated with the hard UV continuum, and is representative of the degree of recent star-formation in the galaxy. The sequence traced in Fig. 13 is similar in shape to the BPT diagram for galaxy line ratios (Baldwin, Phillips & Terlevich 1981). In this diagram, the two reddening-insensitive ratios of $[OIII]/H\beta$ versus $[NII]6584/H\alpha$ discriminate among emission-line galaxies according to the ionization mechanism, i.e., ionization due to ultraviolet radiation of hot stars or to a power-law continuum (Veilleux & Osterbrock 1987).

In the BPT diagram for more than 55,000 galaxies from the Sloan Digital Sky Surveys (Kauffmann et al. 2003, Fig. 1) the star-forming galaxies lie on a tight sequence. This sequence is correlated with the ionization parameter and the metallicity, for which the ratio $[NII]6584/H\alpha$ is a direct estimator (Denicolo' et al 2002).

We checked if the similarity in shape reflects a correlation of the principal components with the line ratios of the BPT diagnostic diagram. Spectroscopic data are available for only very few galaxies, mainly from Terlevich et al. (1991). A correlation with the metallicity can be excluded, while no conclusive relation with the $[OIII]/H\beta$ ratio can be deduced from so few points.

If the sequence in Fig. 13 is tracing the starbursting activity, it should correlate with the luminosity of the Balmer $H\alpha$ line, which is a direct estimator of the presence of young massive stars (Kennicutt 1998). We found in the literature the $H\alpha$ equivalent width (EW) for a few galaxies of this sub-sample and we plotted in Fig. 14 the retrieved values versus the third component values. Although visually there is a hint of a possible correlation, its statistical significance is very low. More such observations and dust attenuation correction are necessary before establishing such expected correlation. However, the ability of the PCA method to separate different contributions to the SEDs could be used as a tool for tracing sequences in larger samples of starburst galaxies.

The data set used was analyzed without any preliminary selection, except for the objective coverage factor, defined in section 2. We specifically avoided any attempt to divide the

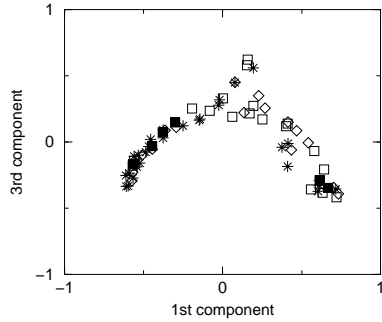


Figure 11. Projections onto the plane defined by the first and the third eigenvectors of the spectra of the normalised and S/N selected sample. Filled squares indicate elliptical galaxies, open squares represent spirals, diamonds irregulars, and stars BCD, HII and compact ones.

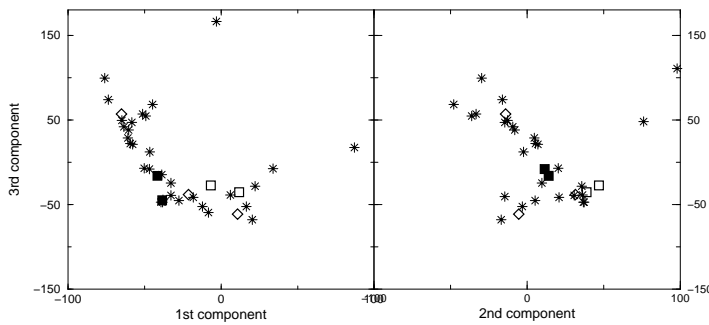


Figure 12. Projections of the spectra of the sub-sample with coverage parameter $C \leq 1$ onto a) the plane defined by the first and the third eigenvectors and b) the plane defined by the second and the third eigenvectors. Filled squares indicate elliptical galaxies, open squares the spiral, diamonds the irregulars, and stars the BCD, HII and compact ones

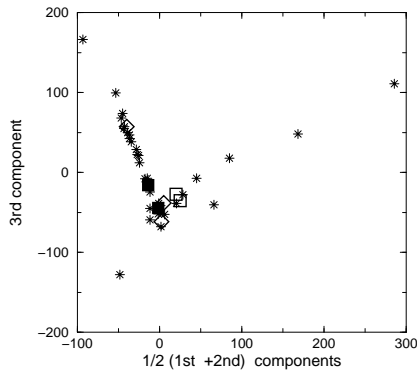


Figure 13. Projections into the plane defined by the linear combination of the first and the second eigenvectors, and the third eigenvectors of the spectra of the sub-sample with coverage parameter up to 1. Filled squares indicate elliptical galaxies, open squares the spiral, diamonds the irregulars and stars the BCD, HII and compact ones

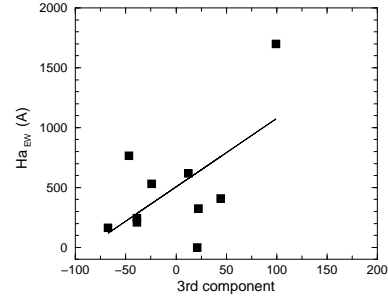


Figure 14. The third component versus $H\alpha$ for some of the compact galaxies. The line shows a linear regression.

sample into sub-groups according to their spectrum, because in the UV some signatures for the presence of young stars are expected for all Hubble types. It is well-known that episodes of star formation occur in a variety of environments, such as nuclei of spiral galaxies, or blue compact galaxies, or HII galaxies or regions.

We searched for an objective parameter that could define a sequence in the UV by projecting the spectra into the principal components plane, such as that found in the optical domain (Connolly et al. 1995; Folkes et al. 1996; Galaz & de Lapparent 1998). The UV domain was included only in the analysis of ten templates by Connolly et al. (1995). However, the UV portion of the SED has a small weight in the spectral range of frequencies analysed (from 1200\AA to $1\mu\text{m}$), and the spectral sequence outlined by the PCA for this sample, is essentially defined by the optical emission of the galaxies.

In our data set, the small size of the entrance aperture of the *IUE* could be one of the causes of the failure of tracing an ordered and continuous sequence of the projections of spectra into the new axes. This aperture sampled only the emission from the optical centre of the light, while often the brightest part of the UV image of a galaxy is rather distant from the centre. In nearby spiral galaxies, for instance, the *IUE* sampled essentially the bulge emission and only partially the disc emission. Since the circum-nuclear bulge hosts a variety of components, including star-forming rings or resolved star clusters and spiral structures (Boker et al. 2001), it is not surprising that many objects classified as spiral galaxies and compact or BCD galaxies populate the same region in the plane of the principal components (see figs. 9, 10)

CONCLUDING REMARKS

In this paper we analyzed the UV spectral energy distribution of normal galaxies listed in the *IUE* INES Guide No. 2-Normal Galaxies (Formigginì & Brosch, 2000) using a Principal Component Analysis. Since this method can reveal the internal correlations of a set of data and retrieve their common features, we aimed to identify an objective parameter able to define a galaxy sequence in the UV.

The sample consists of the SW-*IUE* spectra of the central regions of 118 galaxies, covering a wide range of Hubble types, where the aperture included more than 1 per cent of the galaxy area. The PCA method was applied to the sample without normalisation or scaling, to a sub-sample of good

S/N spectra, normalised by the scalar product, and to a sub-sample where the *IUE* aperture contained more than 10 per cent of the optical galaxy area. The principal components retrieved by the PCA have been associated with the main components observed in the UV spectra of galaxies. The first component, accounting for the largest source of diversity, can be associated with the UV continuum emission. The second component, rising redward of 1500Å, represents the UV contribution of an underlying evolved stellar population (A stars and later). The third component is sensitive to the amount of activity in the central regions of galaxies and measures the strength of recent or current star formation events.

In all the sample and the sub-samples analysed, the principal component representative of star-forming activity accounts for a significant percentage of the variance. In the entire sample, the first three principal components explain 83 per cent of the variance among the spectra.

The fractional contribution to the SED by the evolved stars and by the young population are similar.

The projection of the spectra on the plane defined by the first and the third components for the entire sample fails to outline a regular pattern. For all the morphological types, a contribution from a young population seems to be present in the nuclear region of the galaxies, although with a different activity state. However none of the principal components is able to outline an internal correlation or to correlate with the optical morphological types.

In a sample of 76 good S/N spectra, normalised by the scalar product, the projected spectra show an arc-like sequence, similar to that found by Connolly et al. (1995) for the ten template spectra from the Kinney et al. (1993) sample although with a large overlap of morphological classes.

A reduced sample of 43 galaxies, where the *IUE* aperture included more than 10 per cent of the galaxy, contains almost only compact and BCD galaxies. The projections of the spectra of this sample onto the plane defined by the first and the third principal components outline a sequence that could be related to the degree of starburst activity of the galaxy, where the most active galaxy is Pox 186 and the few early and late-type galaxies occupy the low-activity region. A similar sequence is shown by the projections onto the second and third components. A quasi-monotonic sequence is outlined by the third component with respect to a linear combination of the first and second components. The correlation of the third component with the H α EW is not statistically significant, due to the small number of points. We suggest that more observations could establish that the third principal component indeed represents the star-forming activity of the galaxy.

We initiated this study as an attempt to predict the UV SED using the morphological classification of a galaxy and its optical emission properties, using the *IUE* spectra as the data base. The work described here indicates that some degree of success in this endeavor could be expected, provided that the UV data are based on good signal-to-noise UV spectra that represent the total UV emission of a galaxy.

Assuming that a characterization of the UV properties would be done from the *GALEX* results, the galaxy coverage would be taken care of automatically by using the objective prism feature. However, one would have to deal with low-resolution spectra even for point-like objects ($\simeq 10\text{\AA}$ at

CIV $\lambda 1550$, more than twice that used here) and it is not clear how this would influence the results. Given the lack of spectral discriminators longwards of $\simeq 2000\text{\AA}$, it is unlikely that the LW part of the *GALEX* spectra would add much information content to a future PCA analysis.

Table 1. Table 1- List of galaxies

Id.no.		α_{2000}	δ_{2000}	Coverage	B_T	z	Morph. Type
NGC7828	1	00 06 27	-13 24 54	1.45	14.37	0.01935	Sc
NGC118	1	00 27 16	-01 46 48	1.34	14.63	0.03753	I0
ESOB350-IG38	1	00 36 53	-33 33 14	0.00	15.45	0.02053	S?
ABCG85		00 41 51	-09 18 15	1.92	14.50	0.05567	cD;SB0
ESOB474- 26		00 47 08	-24 22 14	1.78	14.94	0.05271	SA
IC1586	1,2	00 47 56	+22 22 28	0.00	14.90	0.01942	Compact
AOO PKS0123-16	1,2	01 25 48	+01 22 18	0.00	14.42	0.01875	I
MRK2	1	01 54 53	+36 55 02	1.42	13.92	0.01875	SB0a
NGC835	1	02 09 25	-10 08 09	1.91	12.97	0.01359	SAB
IC214	1	02 14 06	+05 10 32	0.00	14.68	0.03022	S
NGC992	1	02 37 26	+21 05 55	1.60	15.56	0.01381	S?
MRK600	1,2	02 51 04	+04 27 09	0.70	14.99	0.00336	SBb;BCD
ABCG400A		02 57 42	+06 01 38	1.20	13.86	0.02215	E
AOO SBSG 0335-052	1,2	03 37 47	-05 02 47	0.46		0.01349	EmLS
ESOB156-IG7		03 41 12	-54 00 39	1.06	15.71	0.05306	G
NGC1510	1	04 03 33	-43 24 01	1.76	13.51	0.00304	SA0
AOO TOL 0420-414	1,2	04 21 59	-41 19 21	0.00	18.26	0.01993	EmLS
AOO TOL 0440-381	1,2	04 42 08	-38 01 03	0.00	18.26	0.04100	EmLS
MRK1094	1	05 10 48	-02 40 54	1.42	13.87	0.00944	I0 pec?
AOO TOL 0513-393	2	05 15 20	-39 17 41	0.00	17.41	0.05000	EmLS
AOO 0644-741		06 43 00	-74 14 11	1.93	13.88	0.02170	E
AOO TOL 0645-376	2	06 46 49	-37 43 25	0.00	17.38	0.02600	EmLS
MRK7	1	07 28 11	+72 34 20	1.31	14.44	0.01021	S
IC2184	1	07 29 25	+72 07 41	0.00	14.38	0.01202	S
AOO HARO 1	1	07 36 57	+35 14 33	1.71	12.72	0.01262	Im?
MRK12	1	07 50 48	+74 21 32	1.80	13.11	0.01318	SAB
PG 0833+652	1,2	08 38 23	+65 07 16	0.00		0.01911	pec HII
NGC2623		08 38 24	+25 45 01	0.00	13.99	0.01846	S
AOO T 0840+120	1,2	08 42 21	+11 50 01	0.00		0.03000	G
MRK702	1	08 45 34	+16 05 48	1.34	15.57	0.05280	Compact
NGC2684		08 54 53	+49 09 38	1.66	13.65	0.00954	S?
NGC2773	1	09 09 44	+07 10 26	1.12	14.46	0.01834	S?
IC2458	1,2	09 21 29	+64 14 11	0.80	15.41	0.00512	I0 pec
MRK116 A	1,2	09 34 02	+55 14 25	0.00	15.61	0.00248	Compact
ESOB435-IG20	1	09 59 21	-28 07 54	1.48	14.40	0.00237	Sb
MRK25	1	10 03 52	+59 26 11	1.20	14.82	0.00868	Sb?
NGC3125	1	10 06 34	-29 56 10	1.69	13.47	0.00288	S:BCDG
MRK26	1,2	10 11 51	+58 53 31	0.58	15.99	0.03043	Sc
MRK33	1	10 32 31	+54 23 56	1.75	12.98	0.00487	Im
NGC3353	1	10 45 23	+55 57 33	1.91	13.22	0.00315	BCD
MRK153	1	10 49 05	+52 19 58	1.40	14.98	0.00805	Scp
MRK1267	1	10 53 04	+04 37 43	1.20	14.16	0.01932	E?
ABCG1126		10 53 50	+16 51 00	0.00	15.12	0.08584	S
NGC3471		10 59 09	+61 31 51	1.93	13.24	0.00710	Sa
AOO APG 148		11 03 54	+40 51 00	0.00		0.03452	G
MRK36	1,2	11 04 58	+29 08 22	0.58	15.64	0.00215	BCD

ACKNOWLEDGMENTS

We acknowledge helpful discussion with O. Lahav and S. Steindling. UV astronomy at Tel Aviv University is supported by the Austrian Friends of the Tel Aviv University.

REFERENCES

- Baldwin, J., Phillips, M., Terlevich, R., 1981, PASP, 93, 5
 Bianchi L. and the Galex team, 1999, Mem.SA.It., 70, 365
 Bica E., Bonatto C., Pastoriza M.G., Alloin D., 1996, A&A, 313, 405
 Boker T., Laine S., van der Marel R.P., Sarzi M., Rix H.W., Ho L.C., Shields J.C., 2002, AJ, 123, 1389
 Bonatto C., Bica E., Alloin D., 1995, A&A, 112, 71
 Bonatto C., Bica E., Pastoriza M.G., Alloin D., 1996, A&AS, 118, 89
 Bonatto C., Bica E., Pastoriza M.G., Alloin D., 1998, A&A, 334, 439
 Bonatto C., Bica E., Pastoriza M.G., Alloin D., 1999, A&A, 343, 100
 Brinchmann J., et al., 1998, ApJ, 499, 112
 Brown T.M., Ferguson H.C., Davidsen A.F., Dorman. B., 1997, ApJ, 482, 685
 Caldwell N., Rose J., Sharples R.S., Bower R.G., 1994, AJ, 106, 473

Id.no.		α_{2000}	δ_{2000}	Coverage	B_T	z	Morph. Type
AOO CASG 816 W	2	11 12 08	+35 52 43	0.40	17.50	0.02844	Compact
MRK170		11 26 50	+64 08 16	1.50	15.03	0.00329	Irr
MCG +13-08-0058	1	11 28 01	+78 59 29	1.85	15.08	-0.00033	Pec
MRK178	1	11 33 29	+49 14 12	0.58	14.45	0.00083	Irr
AOO ARP 248B	1	11 46 45	-03 50 54	1.68	15.15	0.01724	SBb
NGC3991	1	11 57 31	+32 20 00	1.18	13.52	0.01105	Sc
NGC3994	1	11 57 36	+32 16 44	1.58	13.32	0.01040	SA
NGC4004	1	11 58 05	+27 52 38	1.83	13.97	0.01126	Irr
AOO POX 36	1	11 58 59	-19 01 36	1.50	14.28	0.00372	IBm
AOO HE 1203-2644	1	12 05 59	-27 00 54	1.45	14.98	0.00590	HII
IC3017	2	12 09 25	+13 34 25	0.88	14.82	0.00658	BCD
AOO VCC 22	2	12 10 24	+13 10 24	-0.20	16.13	0.00564	BCD?
AOO VCC 24	1,2	12 10 36	+11 45 37	0.80	15.10	0.00430	BCD
MCG +01-31-030	1,2	12 15 19	+05 45 42	0.70	14.99	0.00674	E0 pec?
AOO 1214-277	2	12 17 21	-28 02 32	-0.39		0.02600	EmLS
AOO 1214-28	2	12 17 17	-28 02 33	-0.39		0.02600	EmLS
MRK49		12 19 10	+03 51 28	1.42	14.29	0.00509	E pec: H
AOO VCC 562	2	12 22 36	+12 09 28	0.75	16.43	0.00015	BCD
MRK209	1	12 26 16	+48 29 31	1.48	14.65	0.00094	Sm
NGC4449 ₃	1,2	12 28 11	+44 05 40	3.24	9.84	0.00069	IBm HII
NGC4449 ₄	1,2	12 28 11	+44 05 40	3.24	9.84	0.00069	IBm HII
NGC4449 ₅	1,2	12 28 11	+44 05 40	3.24	9.84	0.00069	IBm HII
NGC4449 ₆	1,2	12 28 11	+44 05 40	3.24	9.84	0.00069	IBm HII
MGC UGC 7905	1	12 43 48	+54 53 45	1.58	14.06	0.01626	S? pec
AOO HARO 33	1	12 44 38	+28 28 19	1.25	12.72	0.00316	S0 pec
NGC4650A		12 44 50	-40 42 54	1.91	13.92	0.00954	S0
NGC4670	1	12 45 17	+27 07 34	1.99	13.07	0.00357	SB0
MCG +02-33-0012	2	12 46 05	+08 28 31	1.00	14.78	0.00495	BCD
AOO TOL 1247-232	1,2	12 50 19	-23 33 57	0.00		0.04800	EmLS
NGC4774	1	12 53 07	+36 49 07	0.00	14.81	0.02793	S
MRK54	1	12 56 56	+32 26 55	1.25	15.29	0.04477	Sc?
NGC4853		12 58 35	+27 35 50	1.61	14.40	0.02555	SA0
QSO 1300+361	2	13 03 03	+35 51 29	0.00	18.00	0.06055	HII
AOO POX 120	2	13 06 42	-12 04 22	0.00	15.70	0.02075	EmLS
AOO POX 124	2	13 07 26	-13 11 01	0.00	15.51	0.02422	EmLS
MCG +07-27-0052	1	13 14 10	+39 08 51	0.00	15.58	0.00388	GPair
MRK450		13 14 48	+34 52 44	1.70	14.33	0.00285	Im?
NGC5122		13 24 15	-10 39 16	1.18	14.10	0.00980	Sc
AOO POX 186	1,2	13 25 51	-11 37 35	0.00	17.00	0.00390	EmLS
MRK66	1,2	13 25 54	+57 15 05	0.88	15.05	0.02176	BCG
NGC5236 ₁	1,2	13 37 00	-29 52 04	3.97	7.92	0.00172	SAB HII
NGC5236 ₃	1,2	13 37 00	-29 52 04	3.97	7.92	0.00172	SAB HII
ESOB383-G44	1	13 37 27	-33 00 22	1.79	14.05	0.01260	SAd
MRK67	2	13 41 56	+30 31 11	0.40	16.36	0.00320	BCD

Calzetti D., Kinney A.L., Storchi-Bergmann, T., 1994, ApJ, 429, 582
 Calzetti D., 1999, Mem.SA.It., 70, 715
 Calzetti D., 2001, PASP, 113, 1449
 Connolly A.J., Szalay A.S., Bershadsky M.A., Kinney A.L., Calzetti D., 1995, AJ, 110, 107
 Corbin R.C., Vacca W.D., 2002, Ap, 581, 1039
 Deharveng J.M., Boselli A., Donas J., 2002, A&A, 393, 843
 De Mello D.F., Leitherer C., Heckman T.M., 2000, ApJ, 530, 251
 Denicolo', G., Terlevich, R., Terlevich, E. 2002, MNRAS, 330, 69
 Doublier V., Kunth D., Courbin, F., Magain, P., 2000, A&A, 353, 887
 Folkes S., Lahav O., Maddox S., 1996, MNRAS, 283, 651
 Formigini L. and Brosch N., 2000, INES Guide No.2: Normal Galaxies- ESA SP-1243, Noordwijk: ESA Publishing Department
 Francis P.J., Hewett P.C., Foltz C.B., Chaffee F.H., 1992, ApJ, 398, 476
 Fricke K.J., Izotov Y.I., Papaderos P., Guseva N.G., Thuan T.X.

2001, AJ, 121, 169
 Galaz G. and de Lapparent V., 1998, A&A, 332, 459
 Gil de Paz, A., Madore, B.F., Pevunova, O., 2003, preprint (astro-ph-0302221)
 Gordon K.D., Clayton G.C., Misselt K.A., Landolt A.U., Wolff M.J., 2003, ApJ, 594, 279
 Heckman T.M., Robert C., Leitherer C., Garnett D.R., van der Rydt F., 1998, ApJ, 503, 646
 Ibata R.A. and Irwin M.J., 1997, AJ, 113, 1865
 Kauffmann, G., et al., 2003, MNRAS, 346, 1055
 Kennicutt R.C., 1992, ApJS, 79, 255
 Kennicutt R.C., 1998, ARA&A, 36, 189
 Kinney A.L., Bohlin R.C., Calzetti D., Panagia N., Wuse R.F.G., 1993, ApJS, 96, 5
 Kuchinski L.E. et al., 2000, ApJS, 131, 441
 Kuchinski L.E., Madore B.F., Freedman W.L., Trewella M., 2001, ApJ, 122, 729
 Kunth, D. and Östlin, G., 2000, A&AR, 10, 1
 Lahav O. et al. 1995, Science, 267, 859

Id.no.		α_{2000}	δ_{2000}	Coverage	B_T	z	Morph. Type
NGC5291		13 47 24	-30 24 27	1.69	13.64	0.01463	E pec:
ABCG1795		13 48 52	+26 35 35	1.80	15.20	0.06326	cD;S0?
AOO Z 13502+0022	1	13 52 44	+00 07 51	1.06	15.43	0.01209	Sm
MCG +04-33-038	1	14 01 09	+21 14 15	1.18	15.04		GPair
AOO TOL 41	2	14 02 59	-30 14 25	-0.30	18.00	0.02308	EmLS
IC4448		14 40 28	-78 48 37	1.70	14.06	0.01543	SBd
MRK288	2	14 50 47	+73 49 24	0.00	15.70	0.02502	S?
MCG +06-33-00 0004	1	14 50 57	+35 34 17	1.75	14.77	0.00405	BCDG
ABCG1991		14 54 32	+18 38 24	1.83	15.29	0.05921	E
AOO CASEG 657	1,2	15 12 13	+47 16 31	0.00	16.30	0.05350	Compact
MRK487	1,2	15 37 04	+55 15 47	0.58	15.46	0.00002	Compact
NGC5996	1	15 46 59	+17 53 08	1.99	13.01	0.01100	SBc
NGC6090	1	16 11 40	+52 27 21	0.75	14.49	0.02930	GPair
MRK499	1,2	16 48 24	+48 42 23	0.40	14.60	0.02567	Im:
AOO FRL 44		18 13 39	-57 43 58	1.10		0.01650	S? pec
ESOB338-IG4	1	19 27 58	-41 34 28	1.31	13.42	0.00959	pec HII
ESOB185-IG13	1,2	19 45 01	-54 15 03	0.88	15.00	0.01868	Compact:HII
ESOB462-IG20	1	20 26 57	-29 07 06	0.00	14.60	0.02011	E
ESOB400-G4	1	20 37 42	-35 29 11	1.10	14.28	0.01968	Compact:HII
NGC7173		22 02 04	-31 58 25	1.83	13.14	0.00833	E pec:
NGC7176		22 02 09	-31 59 25	1.70	12.42	0.00838	E pec
NGC7250	1	22 18 18	+40 33 45	1.93	13.20	0.00389	Sdm?
MCG -07-47-023		23 13 59	-42 43 39	1.82	15.51	0.05640	SA0
NGC7609 B		23 19 31	+09 30 10	1.27	16.00	0.03857	Sm
ABCG2597		23 25 20	-12 07 27	1.40	16.32	0.08220	Elliptical
NGC7673	1	23 27 42	+23 35 24	1.99	13.10	0.01137	SAc? pec
AOO Z 2327.6+251	1	23 30 09	+25 31 43	0.69	15.06	0.01923	Sb
ABCG2626	2	23 36 30	+21 08 48	0.70	15.31	0.05499	S0
ABCG2634		23 38 30	+27 01 51	0.00	13.47	0.03022	E

Longo G. and Capaccioli M., 1992, "*IUE* ULDA Access Guide No.3: Normal Galaxies", ESA SP-1152

Mass-Hesse, J.M. and Kunth, D., 1998, in "Ultraviolet Astrophysics: Beyond the *IUE* Final Archive" ESA SP-413, pag 537

Mittaz J.P.D., Penston M.V., Snijders M.A.J., 1990, MNRAS, 242

Östlin G. & Kunth D., 2001, A&A, 371,429

Papadopoulos P., Izotov Y., Fricke K.J., Thuan T.X., Guseva N.G., 1998, A&A, 338, 43

Ronen S., Aragon-Salamanca, A., Lahav O., 1999, MNRAS, 303,284

Seaton M.J., 1979, MNRAS, 187,73

Singh H. P., Gulati R.K., Gupta R., 1998, MNRAS, 295, 312

Sodré L. and Cuevas H. ,1994, Vistas in Astronomy, 38,287

Sodré L. and Cuevas H. ,1997, MNRAS, 287,137)

Steindling, S., Brosch, N. and Rakos, K.D., 2001, ApJS, 132, 19

Terlevich R., Melnick J., Masegosa J., Moles M., Copetti M.V.F., 1991, A&AS, 91, 285

Turler M. and Courvoisier T.J.-L., 1998, A&A, 329, 863

Veilleux, S & Osterbrook D.E., 1987, ApJS, 63,295

Whitney C.A., 1983, A&AS,51,443